Int. J. Nanoelectronics and Materials **4** (2011) 121-134

Structural, electrical and optical properties of *N*-(*p* dimethylaminobenzylidene)-*p*-nitroaniline thin films

E. M. El-Menyawy[1,*], H. M. Zeyada[2], M. M. El-Nahass[3]

[1]*Solid State Physics Department, Solid State Electronics Lab, National Research Center, Dokki, Cairo, 12622 Egypt.*
[2]*Physics Department, Faculty of Science at Damietta, 34517 New Damietta, Egypt.*
[3] *Physics Department, Faculty of Education, Ain Shams University, Roxy, Cairo,11757 Egypt.*

Received 22 July 2010; Accepted 9 Nov. 2010

Abstract

Structural, direct current (DC) electrical and optical properties of thermally evaporated *N*-(*p*-dimethylaminobenzylidene)-*p*-nitroaniline (DBN) thin films have been studied. The crystal structure of DBN in both powder and thin film forms is determined by the X-ray diffraction technique. The results showed that the material is polycrystalline in both powder and as-deposited thin films. The DBN in powder form has a triclinic crystal structure with a space group of *P*1. The crystallite size of the films is calculated as a function of both film thickness (250-1100 nm) and annealing temperatures (353,373 and 393 K). The resistivity of DBN thin films is measured as a function of film thickness. The temperature dependence of DC electrical conductivity for DBN films is calculated with different film thickness. The temperature dependence of DBN thin films showed a typical semiconductor behavior. The films have two activation energy of conduction in the temperature range of (303-393 K). The two activation energies decease with increasing film thickness. The absorption coefficient and the optical band gap are estimated for DBN films.

Keywords: Organic thin films; Structural properties; Electrical properties.
PACS: 71.20.Rv, 73.61.Ph, 78.30.Jw.

1. Introduction

There has been a considerable interest in organic materials exhibiting a semi-conducting character because of their importance in many low-cost technological applications such as organic light emitting diodes, sensors and photovoltaic cells [1]. They have the key advantage of simple and low-temperature thin film processing through inexpensive techniques such as spin and dip coatings, ink-jet printing, or stamping [2]. In addition, the flexibility of organic chemistry enables the creation of organic molecules with specific optical and electrical properties.

The *N*-(*p*-dimethylaminobenzylidene)-*p*-nitroaniline (DBN) is one of the Schiff bases compounds, which posses many technological applications [3-7] such as: molecular switch, temperature indicator devices, temperature sensitive light filters, imaging systems

[*]) For correspondence, Tel: + 20106021326, Fax: + 20233709310, Email: emad_elmenyawy@yahoo.com.

and storage of energy. The DBN compound is also one of the benzylideneaniline derivatives, which has donor and acceptor groups (dimethylamino and nitro groups, respectively), the electronic properties of such compounds received a great deal of attention [8, 9]. The DBN compound was found in four polymorphs [10, 11] depending on the solvent which was used in the re-crystallization process; all these studies verified that the molecule has non-planar structure in these forms. The AC electrical conductivity and dielectric properties of DBN thin films sandwiched between two gold electrodes were studied by the authors [12]. The results showed that the correlated barrier hopping is the operating conduction mechanism in the temperature range starting from room temperature up to 393 K.

The application of the DBN in any one of the above mentioned devices will certainly be provided as thin films. The parameters controlling the physical properties of thin films are: structure [13, 14], composition [15, 16], film thickness [17, 18] faults probability [19] and the presence of impurities [20]. The annealing and substrate temperatures are considered as processing variables that are used to influence structural parameters such as volume fraction of crystallized and second phase, grain size and its shape and inter-particle spacing.

To the best of our knowledge, structural, DC electrical and optical properties of thermally evaporated DBN thin films have not yet been reported, so in this work, we aim to investigate the effect of some environmental parameters (film thickness and annealing temperature) on the structural and the DC electrical properties of DBN thin films. The type of electronic inter-band transition, optical band gap and Urbach energy are also determined for the films.

2. Material and Experimental Procedures

The powder used in this study was prepared by direct condensation of *p*-nitroaniline (purity of 99%) and *p*-dimethyleaminobenzaldehyde (purity of 99%), which were obtained from Aldrich Company. The powder was purified by the re-crystallization from acetone solution. The molecular structure of the DBN compound is shown in Fig. 1.

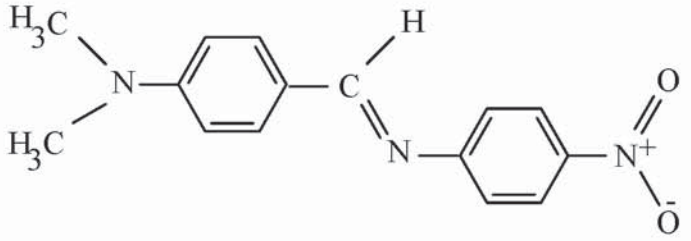

Fig. 1: Molecular structure of DBN.

Thin films of different thickness were prepared by conventional thermal evaporation technique using a high vacuum coating unit (Edward 306 A, England). The films were deposited onto well-cleaned glass substrates for the X-ray diffraction XRD experiments and electrical measurements. The films were vacuum deposited from the powder by using a quartz crucible source heated slowly by a molybdenum boat in a vacuum of 2×10^{-4} Pa. During deposition, the substrates were kept at room temperature. The films were air annealed at 353, 373, and 393 K for the structural determination and only at 373 K with a soaking time of one hour for the electrical measurements.

The film thickness and deposition rate were measured during the evaporation by using a quartz crystal thickness monitor (Model, TM-350 MAXTEK, Inc.). The deposition

rate was controlled at about 2 Å/s. After deposition, the film thickness was also checked interferometrically [21].

The X-ray diffractometer (Philips X" pert, Pro.) with Ni-filtered CuK_{α}-radiation was used to study the structural properties of DBN in both the powder form and the thin film forms in the range of diffraction angle, 2θ, (4-60°). The applied voltage and the tube current were 40 KV and 30 mA, respectively.

The two-point probe technique was used in measurements of DC electrical resistivity and conductivity of DBN thin films with different thickness in planar structure. The ohmic contacts at the two ends of DBN thin films were provided by thermal evaporation of pure gold. The resistance of the DOPNA film as a function of temperature was measured in the range (303-393 K) using high impedance Keithly 617 programmable electrometer. The temperature of the sample was recorded during the electrical measurements by using NiCr-NiAl thermocouple with accuracy of ±1 K. All measurements were performed at different temperatures in air and under dark conditions.

A double beam spectrophotometer (JASCO model V-570 UV-VIS-NIR) was used to measure the absorbance A(λ) at the normal incidence of the light. The relative uncertainty for absorbance given by manufacturer is ±1%.

3. Results and Discussion

3.1. Structural Analysis

The X-ray diffraction patterns of DBN in powder form and for the as-deposited thin film of thickness 250 nm is shown in Fig. 2. The results show that there are several peaks with different intensities indicating that the material is polycrystalline in both forms. A relatively few number of reflections with small peak amplitude is observed in (XRD) pattern of thin film in comparison with the XRD pattern of powder form is a result of small number of unit cells in thin film.

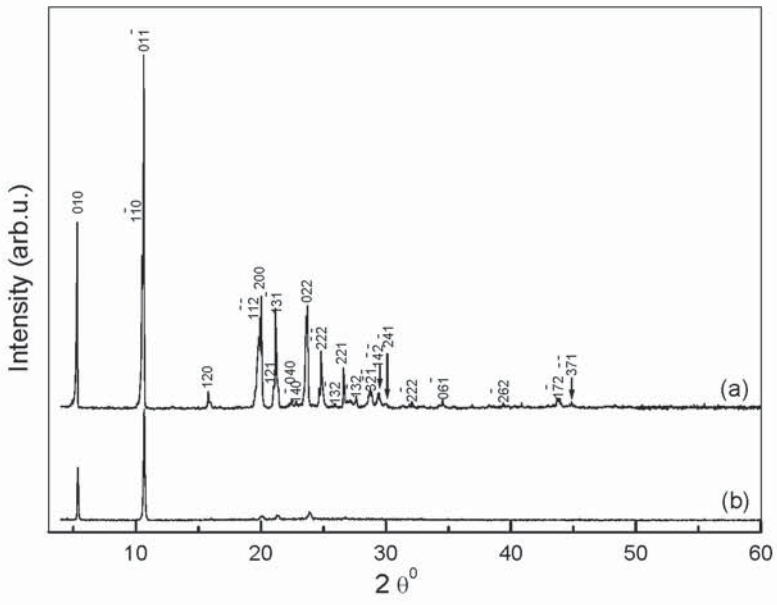

Fig. 2: X-ray diffraction pattern of DBN compound: (a) is the powder form and (b) is the as-deposited thin film with a thickness of 250 nm.

All the diffraction peaks of DBN in the powder form are indexed and the lattice parameters are determined with the aid of CRYSFIRE computer program [22]. The values of inter-planar spacing, *d*, and Miller indices, *hkl,* for each diffraction peak before and after refinement are determined by using CHEKCELL program [23]; and they are listed in Table 1. The results showed that DBN compound has a triclinic crystal structure and the lattice parameters are: a = 9.55084 Å, b = 9.5221Å, c = 16.2189 Å, α = 100.97°, β = 91.60°, γ =107.45°, with a space group $P1$. These results are in well agreement with that reported by Nakai et al. [10] for DBN single crystal. In that analysis, the lattice parameters for DBN were determined as: 9.509 Å, 9.505 Å, 16.200 Å, 101.04°, 91.69° and 107.52°), with a space group $P1$ in which the DBN crystals were obtained by re-crystallization from acetone as a solvent.

Table1: Comparison between the measured and the calculated inter-planar spacing of DBN powder.

No.	2θ°	d_{exp}	d_{cal}	(hkl)
1	5.285	16.706	15.831	010
2	10.473	8.439	8.538	$\bar{1}10$
3	10.624	8.319	8.174	$0\bar{1}1$
4	16.684	5.309	5.370	120
5	19.789	4.482	4.480	$\bar{1}\bar{1}2$
6	20.055	4.423	4.432	200
7	21.192	4.188	4.175	121
8	21.380	4.152	4.146	$\bar{1}31$
9	22.467	3.953	3.957	040
10	22.808	3.895	3.935	$\bar{1}40$
11	23.594	3.767	3.771	022
12	23.747	3.743	3.755	$0\bar{4}1$
13	24.828	3.583	3.582	$\bar{2}\bar{2}2$
14	26.633	3.344	3.331	221
15	27.637	3.224	3.218	$\bar{1}32$
16	28.715	3.106	3.102	$\bar{3}\bar{2}1$
17	29.448	3.030	3.035	$\bar{1}\bar{4}2$

18	30.044	2.971	2.969	$\bar{2}41$
19	32.130	2.783	2.773	$\bar{2}22$
20	34.557	2.593	2.598	$0\bar{6}1$
21	39.395	2.285	2.282	$\bar{2}62$
22	43.761	2.066	2.068	$\bar{1}72$
23	44.809	2.020	2.020	$\bar{3}\bar{7}1$

The influence of the film thickness range (250-1100 nm) on the XRD pattern of DBN films is shown in Fig. 3. The results show that the integrated intensity of the peaks increases with increasing film thickness; this indicates that the crystallite size varies with increasing film thickness in the considered range.

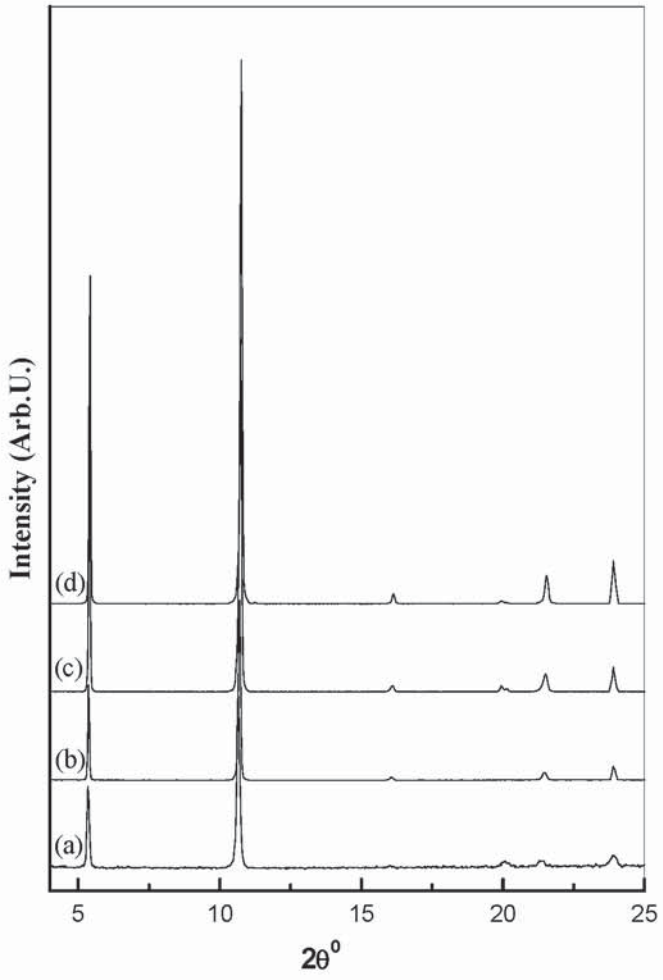

.Fig. 3: X-ray diffraction pattern of the as-deposited DBN thin films with different thickness: (a) 250 nm, (b) 450 nm, (c) 700 nm and (d) 1100 nm.

The crystallite size, CS, can be calculated from (XRD) pattern using Scherrer formula [24]:

$$CS = \frac{n\lambda}{\beta \cos\theta} \tag{1}$$

where n is the scherrer's constant and was taken as 0.9, λ is the wavelength of the X-ray, β is the full width at half maximum of the obtained peak corrected for instrumental broadening and θ is the diffraction angle.

The value of the crystallite size is calculated at the most intense peak ($2\theta \approx 10.615^{\circ}$) of the films for the different film thickness, and it is shown in Fig. 4. The crystallite size increases non-linearly with increasing film thickness.

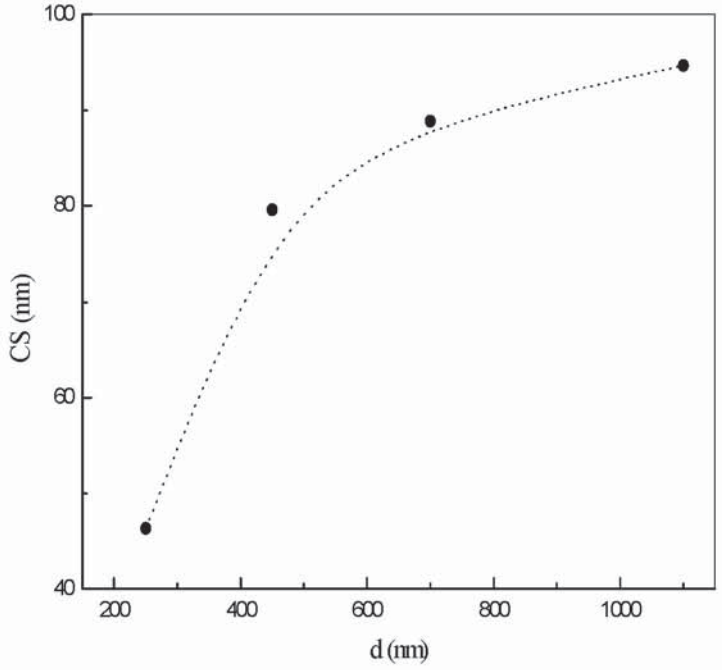

Fig. 4: Calculated crystallite size determined at the most intense peak ($2\theta \approx 10.615^{\circ}$) vs. the film thickness.

The influence of annealing temperatures (353,373 and 393 K, soaking time is one hour) on the XRD pattern of DBN thin film with film thickness of 250 nm is shown in Fig. 5. The figure shows also that integrated intensity of the peaks increases with increasing annealing temperature. The crystallite size determined using Eq. (1) at the most intense diffraction peak ($2\theta \approx 10.615^{\circ}$) as a function of annealing temperature is shown in Fig. 6. The value of the crystallite size increases also non-linearly with increasing annealing temperature.

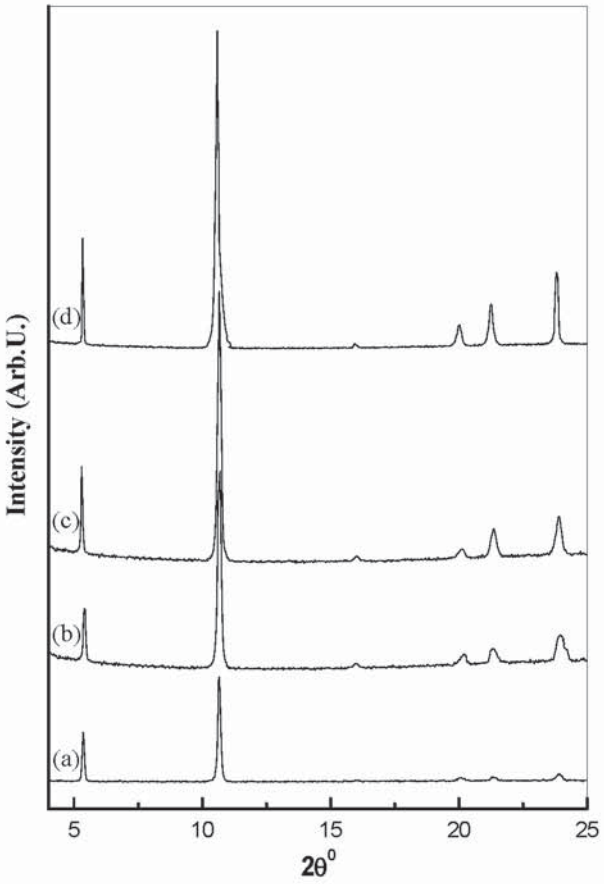

Fig. 5: X-ray diffraction pattern of DBN thin film with a thickness of 250 nm annealed at different temperatures: (a) as deposited, (b) at 353 K, (c) at 373 K and (d) at 393 K.

3.2 DC Eelectrical Resistivity

The DC electrical resistivity, ρ, of the DBN films in planar configuration with two gold electrodes is calculated from the measured resistance data using the film dimensions. The measurements of dark electrical resistivity as a function of film thickness, d, for the as-deposited and annealed films at 373 K are depicted in Fig. 7. Inspection of this figure shows that the resistivity decreases non-linearly with increasing film thickness. This decrease in resistivity continues up to reach a relatively constant value at thicker films at which the structure of the films approaches that of the bulk material, this behavior is observed for organic [25] and inorganic [26] materials which can be explained on the bases of Seto's model [27] of polycrystalline materials. In that model, the mobility of charge carriers increases with increasing the film thickness due to increasing the grain size.

Fig. 7 shows also that, the electrical resistivity of the annealed films is lower than that for the as-deposited ones; this is again attributed to increasing the crystallite size caused by annealing as it was shown previously in Fig. 6.

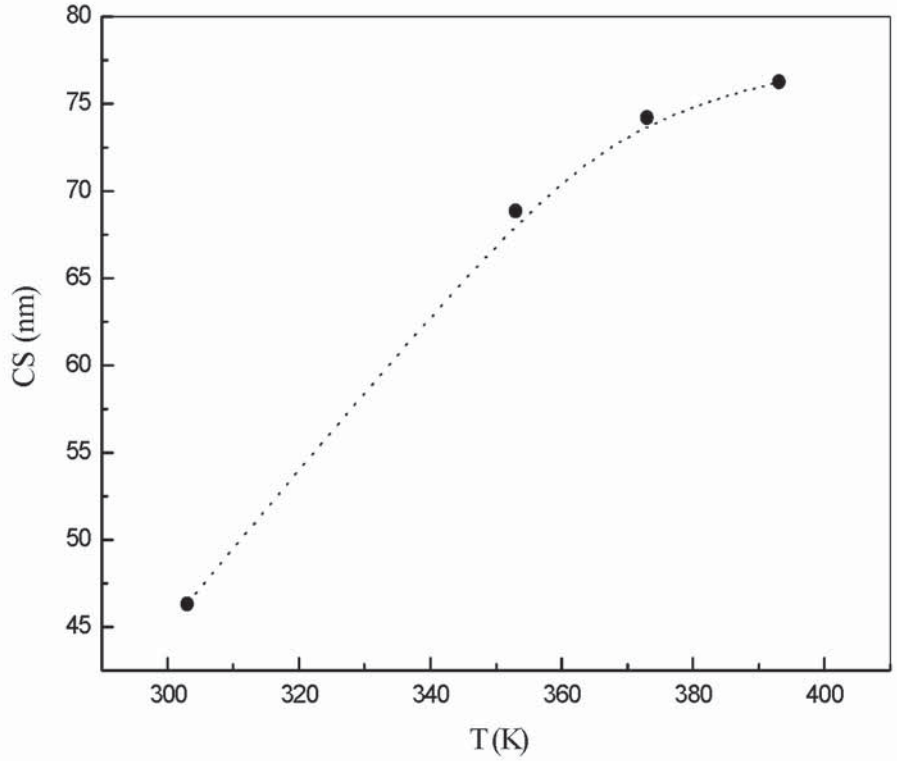

Fig. 6: Calculated crystallite size determined at the most intense peak ($2\theta \approx 10.615^{\circ}$) vs. the annealing temperatures.

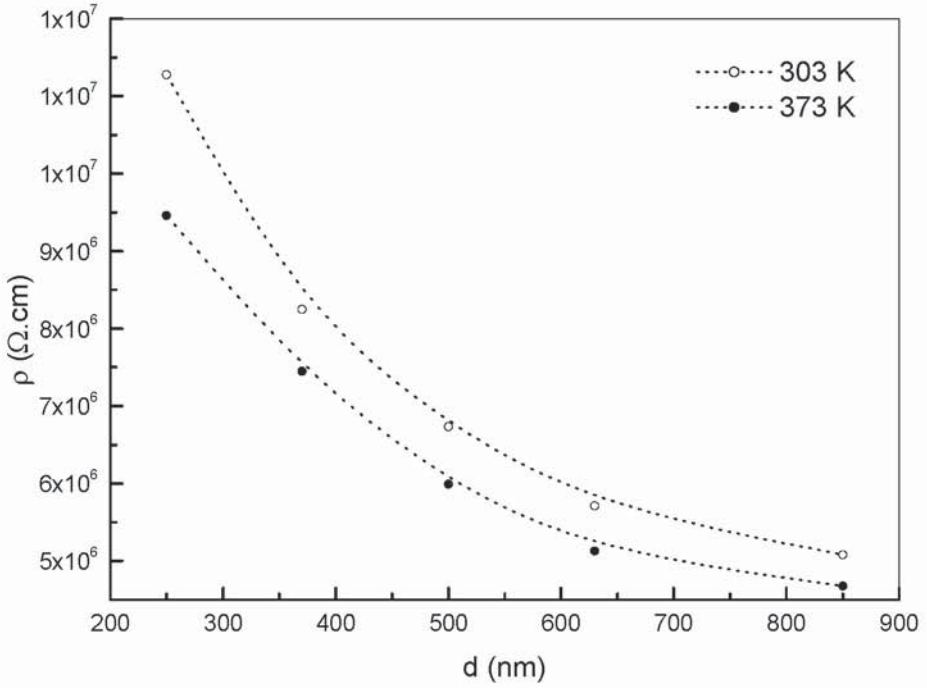

Fig. 7: The variation of Ln σ as a function of temperature for DBN thin films with different thickness.

3.3 Dark Electrical Conductivity as A Function of Temperature

Electrical conductivity is a prominent factor which reveals reliable information about the transport phenomenon. Fig. 8 shows the variation of natural logarithm of DC conductivity versus the inverse of temperature for different DBN film thickness. It is observed that for each film thickness, the conductivity increases as the temperature increases which may be due to increasing the concentration and/or the enhancement of the mobility of the charge carriers. This indicates a semi-conducting nature of DBN thin films. The relation exhibits two linear portions depending on the temperature range in which the measurements are performed. The conductivity shows thermally activated process and can be analyzed by an Arrhenius equation of the form [28]:

$$\sigma_{DC} = \sigma_o \exp(\frac{-E_a}{kT}) \tag{2}$$

where σ_o is the pre-exponential factors, E_a is the activation energy for this thermally activated process, T is the absolute temperature and k is the Boltzmann constant.

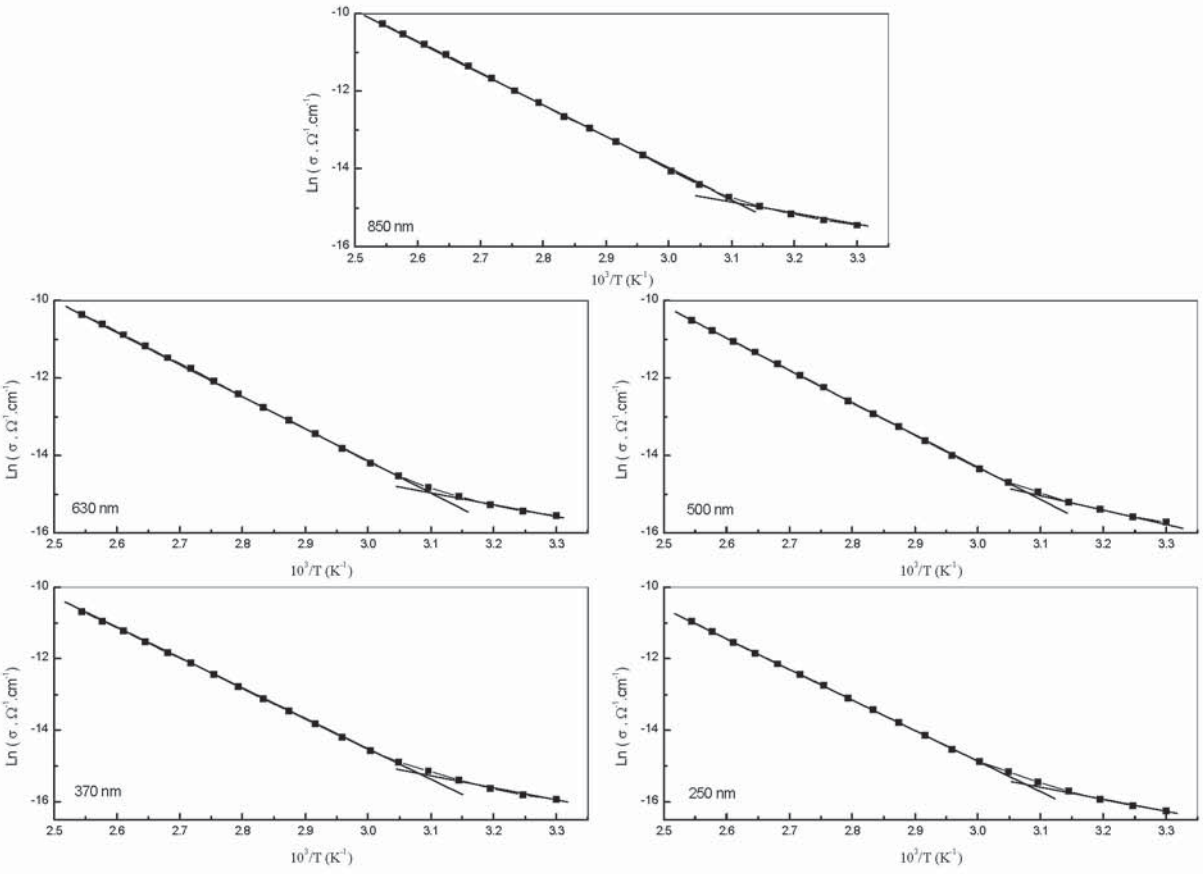

Fig. 8: The variation of the measured resistivity at 303 K as a function of film thickness for the as deposited and annealed DBN thin films at 373 K.

The curves exhibits two activation energies denoted by E_{a1} at relatively low temperatures and E_{a2} at relatively higher temperatures. The activation energies are calculated and listed in Table 2. Observations of this table show that the activation energy decreases slightly with increasing film thickness which is a result of increasing the grain size. At the low temperatures (303-323 K) of the investigated film thickness range, the average activation energy in this range is equal to 0.27 eV. At relatively high temperatures (323-393 K), the average value of activation energy is equal to 0.72 eV. In the first part (within lower temperature range), the organic compounds probably possess an extrinsic conduction, while in the next portion, with a larger slope, the semiconductors exhibit an intrinsic conduction [29].

Table 2. The dependency of activation energies on DBN film thickness.

Film thickness (nm)	Activation energy (eV)	
	E_{a1}	E_{a2}
850	0.27	0.71
630	0.27	0.72
500	0.29	0.72
370	0.30	0.73
250	0.303	0.74

To examine that the conductivity in the relatively high temperature conductivity is due to intrinsic conduction, the absorbance spectra of DBN thin film with a thickness of 440 nm is recorded and the absorption coefficient, α, for the film is calculated by the equation of the form [30]:

$$\alpha = \frac{\ln 10}{\mathrm{d}} \boldsymbol{Abs} \tag{3}$$

where d is the film thickness and ***Abs*** is the absorbance. The variation of the absorption coefficient with the photon energy for DBN thin film is shown in Fig. 9(a). The DBN film has an absorption coefficient in the order of 10^4 cm^{-1}. For the incident photon energy greater than the band gap of semiconductors, the optical absorption usually follows the power law given by [31]:

$$\alpha h\nu = C\left(h\nu - E_g\right)^m \tag{4}$$

where m =1/2 and 3/2 for direct allowed and forbidden transitions, respectively; m=2 and 3 for indirect allowed and forbidden transitions, respectively, $h\nu$ is photon energy and C is a parameter depending on transition probability.

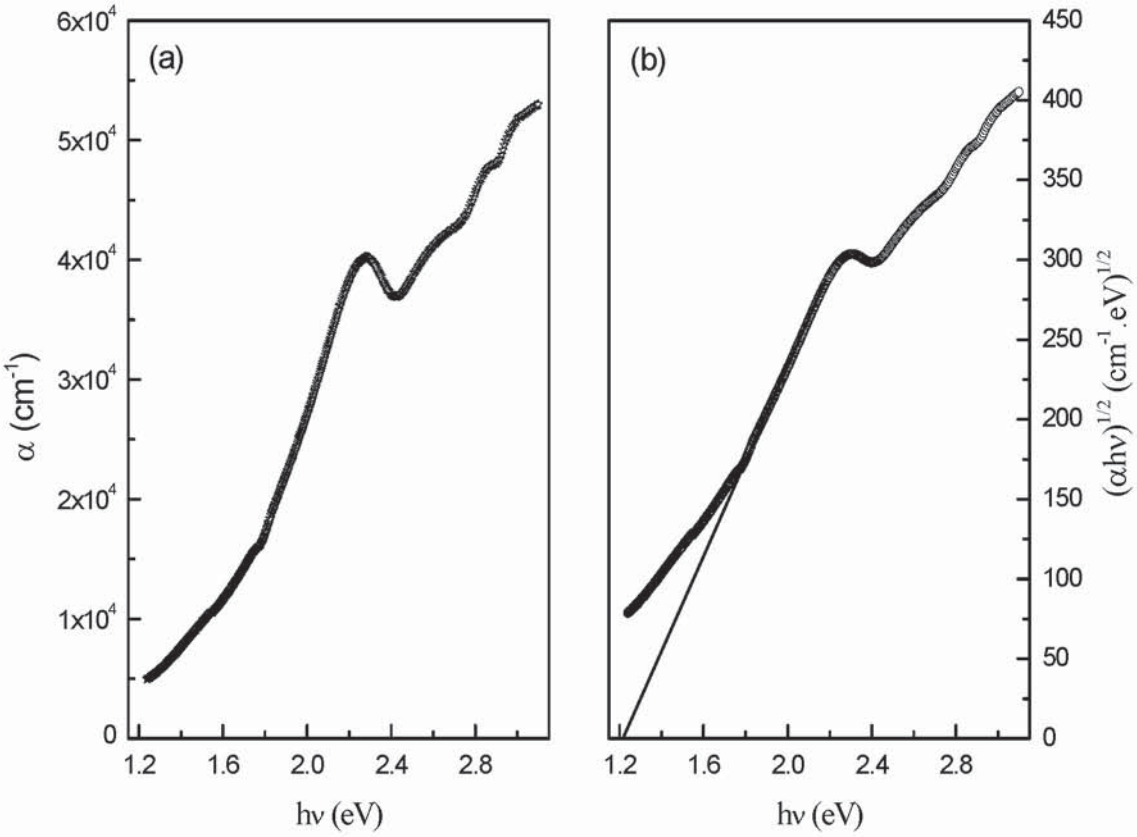

Fig. 9: (a). The absorption spectrum of as-deposited DBN thin films with a thickness of 440 nm., (b) The variation of $(\alpha h\nu)^{1/2}$ as a function of the photon energy for as-deposited DBN thin films with a thickness of 440 nm.

The absorption coefficient data has been fitted with the above theoretical equation for different values of the exponent *m*. The results showed that the films have indirect allowed transition. The relation between $(\alpha h\nu)^{1/2}$ and hν for as-deposited DBN thin film is illustrated in Fig. 9(b). The value of the optical energy gap of the as-deposited film is estimated as 1.22 eV. This value of optical band gap is approximately twice the average value of the activation energy (0.72 eV) for the DBN films determined in the temperature range of (323-393 K) supporting, that the intrinsic conduction is the operating mechanism in that region.

The absorption coefficient of DBN thin film which shown in Fig. 9(a) shows an absorption tail in the photon energy less than the optical band gap. The origin of this band tailing is still a matter of conjecture, but according to Dow and Redfield [32], it arises from the random fluctuations of the internal fields associated with structural disorder which are considerable in many amorphous solids.

The amount of tailing can be estimated by plotting the absorption edge data in terms of an equation originally given by Urbach [30]:

$$\alpha = \alpha_o Exp\left(\frac{h\nu}{E_o}\right) \tag{5}$$

where α_o is the absorption coefficient background and E_o is the Urbach energy. The value of E_o is estimated from the slope shown in Fig. 10 as 0.28 eV. The value of E_o is an indicator of structural disorder of amorphous films. The structural disorder is generally due to the configurational disorder, including variation in bond length and bond angles, which adds to medium-range topological disorder and to compositional disorder, altering the distribution of states at band edges and tailing them into the band gap. In the present study, we can suppose that the polycrystalline DBN thin films also contain an amorphous phase, embedded organic crystallites. By other words, the structural disorder is dominated by the presence of grain boundary.

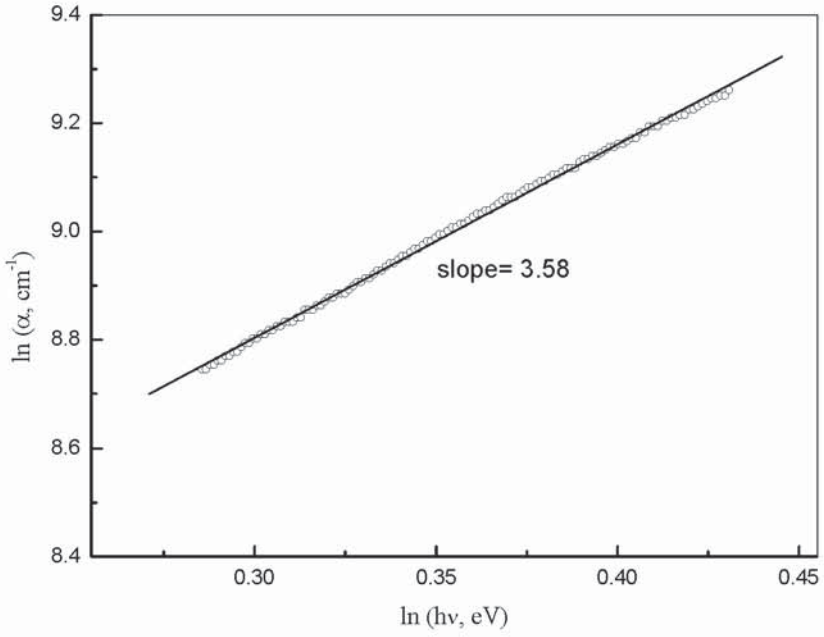

Fig. 10: the relation between ln α and ln hν for as-deposited DBN thin film with a thickness of 440 nm

4. Summary and Conclusion

The main conclusion of the current investigation can be summarized as follows: *N*-(*p*-dimethylaminobenzyli-dene)-*p*-nitroaniline (DBN) in powder form exhibited polycrystalline structure with triclinic crystal system, the lattice parameters are determined as a = 9.55084 Å, b = 9.5221Å, c = 16.2189 Å, α = 100.97°, β = 91.60°, γ =107.45°, with a space group $P1$. Miller indices values for crystal planes of DBN are also determined. The thermally deposited DBN thin films have polycrystalline structure, the crystallite size of such films increases with increasing both the film thickness range (250-1100 nm) and the annealing temperatures range (353,373 and 393 K). The resistivity of Au/DBN/Au thin films (in planer configuration) decreases with increasing both film thickness and annealing temperature (373 K).

The temperature dependence of DC conductivity for DBN thin films showed a typical semiconductor behavior. The relation exhibited two activation energies. The average value of the lower one is determined as 0.27 eV while that of the higher one is given as 0.72 eV. The optical band gap of DBN thin film with a thickness of 440 nm is determined as 1.22 eV, this value is approximately twice the value of the activation energy in the temperature range of (323-393 K) indicating that intrinsic conduction is applicable in that temperature range.

The low optical band gap value for DBN suggests the validity of using these films as a photovoltaic material. The temperature dependence of electrical conductivity as well as the absorption spectra suggests that the model based on band gap representation could be useful for the explanation of the electron transfer mechanism through DBN organic thin films.

References

[1] M. M. El-Nahass, H. M. Zeyada, M. S. Aziz, N. A. El-Ghamaz, Opt. Mater. **27** (2004) 491

[2] J. Gping, T. Tano, Y. Ichino, T. Hanada, Jpn. J. Appl. Phys. **40** (2001) L948

[3] W. H. Fang, Y. Zhang, X. Z. You, J. Mol. struct. Theochem **334** (1995) 81

[4] M. Calligaris, L. Randaccio (Eds), *Comprehensive Coordination Chemistry*, Pergramon, Oxford (1987) 715

[5] L. T. Hee, D. Lavabre, G. Levy, T. C. Micheau, New J. Chem. **13** (1989) 227

[6] K. Sone. Y. Fukuda, *Inorganic thermocromitism*, Springer-Verlag, Berlin (1987)

[7] W. Wueffen, P. M. Theus, Pharmazie **22** (1968) 428

[8] A. C. V. Walree, O. Franssen, A. W. Marsman, C. M. Flipse, W. L. Jenneskens, J. Chem. Soc. **2** (1997) 799

[9] A. C. V. Walree, A. W. Marsman, C. M. Flipse, W. L. Jenneskens, W. L. Jenneskens, W. J. J. Smeets, A. L. Anthony, J. Chem. Soc. **24** (1997) 809

[10] H. Nakai, M. Shiro, K. Ezumi, S. Sakata, T. Kubota. Acta Cryst. B **32** (1976) 1827

[11] H. Nakai, K. Ezumi, M. Shiro, Acta cryst. B **37** (1981) 193

[12] M. M. El-Nahass, H. M. Zeyada, M. M. El-Samanoudy, E. M. El-Menyawy, J. Phys.: Condens. Matter **18** (2006) 5163

[13] J. Rouxel, Chem. Scr. **28** (1988) 33

[14] P. Hagenmuller, Sol. St. Ion. **40–41** (1990) 3

[15] K. Sedeek, E.A. Mahmoud, F.S. Terra, S.M. El Din, J. Phys. D: Appl. Phys. **27** (1994) 156

[16] K. Senthile, D. Mangalaraj, Sa.K. Narayandss, B. Hong,Y. Roh, C.S. Park, J. Yi, Semicond. Sci. Technol. **17** (2002) 97

[17] M. M. El-Nahass, H. M. Zeyada, M. S. Aziz, N. A. El-Ghamaz, J. Opt. Mater. **20** (2002) 159

[18] H. S. Soliman, D. Abdel-Hady, E. Ibrahim, J. Phys.: Condens. Matter. **10** (1998) 847

[19] J. Rouxel, Y. Moelo, A. Lafond, F. J. Disalvo, A. Meerschault, R. Roesky, Inorg. Chem. **33** (1994) 3358

[20] G. A. Wiegers, A. Meetsma, S. Von Smaalen, R. J. Haange, J. Wulf, T. Zeinstra, T. L. DeBoer, S. Kuypres, G. V. Tendeloo, J. V. Landuyt, S. Amelinekx, A. Meerschaut, R. Rabu, J. Roxel, Sol. St. Commun. **70** (1989) 409

[21] S. Tolansky, *Multiple-Beam Interference Microscopy of Metals*, Academic Press, London (1970) 55

[22] R. Shirley, *the CRYSFIRE System for Automatic Powder Indexing: User's Manual*. The Lattice Press, England (2000)

[23] J. Laugier, B. Bochu, LMGP-Suite suite of Programs for the interpretation of X-ray Experiments, ENSP/Laboratoire des Materiaux et du Genie Physique, BP46.38042, Saint Martin d'Heres, France (2000)
[24] B. D. Cullity, *Elements of X-ray Diffraction*, Addison-Wesley Publishing Company, Inc. (2000) 170
[25] M. M. El-Nahass, H. M. Zeyada, A. A. Hendi, Eur. Phys. J. **25** (2004) 85
[26] *ibid*
[27] J. Y. W. Seto, J. Appl. Phys. **46** (1975) 5247
[28] H. M. Zeyada, M. M. El-Nahass, Appl. Sur. Sci. (2007) in press
[29] L. Leontie, M. Roman, F. Brinza, C. Podaru, G. I. Rusu, Syn. Metals **138** (2003) 157
[30] M. M. El-Nahass, H. M. Zeyada, K. F. Abd-El-Rahman, A. A. M. Farag, A. A. A. Darwish, Spectrochimica Acta (2007) in press
[31] J. Tauc, A. Menth, J. Non-Cryst. Solids **8-10** (1972) 569
[32] J. D. Dow, D. Redfield, Phys. Rev. B **5** (1972) 594